The 5th Joint International Conference on Multibody System Dynamics
June 24 – 28, 2018, Lisboa, Portugal

Use of high-order beam element based on the absolute nodal coordinate formulation in the dynamic analysis of rotating shafts

Babak Bozorgmehri[1], Vesa-Ville Hurskainen[1], Marko K. Matikainen[1] and Aki Mikkola[1]

[1]*Mechanical Engineering, Lappeenranta University of Technology, babak.bozorgmehri@lut.fi, vesa-ville.hurskainen@lut.fi, marko.matikainen@lut.fi, aki.mikkola@lut.fi*

ABSTRACT *A finite element method based on the absolute nodal coordinate formulation (ANCF) is applied to the dynamic analysis of high-speed rotors in this stydy. In the ANCF, elements are parameterized by slope vectors in the transversal directions allowing the description of shear and cross-sectional deformations. This study employs a four-node high-order ANCF beam element with derivatives of order three in transversal directions. The element employs one position vector and nine slope vectors at each nodal location. The high-order ANCF beam element is applied to various benchmark tests with circular cross-section structures. As numerical examples demonstrate the beam element is capable of capturing complex cross-section deformation modes more-accurately than the low-order ANCF beam formulations.*

1 Introduction

High-speed motors can be the ideal solution for many pumps, compressors, generators and machine tool systems. There are, however, numerous challenging areas of dynamics associated with the design of high-speed rotating systems. For this reason, the linear theory of rotor-dynamics may not lead to acceptable solutions. It is noteworthy to point out that high-speed rotating machines are subjected to cross-section deformation such as radial expansion, which is proportional to speed of rotation. Significant cross-section deformation mostly occurs in tubular shafts and results from gyroscopic and centrifugal stiffening effects. This may successively influence the stability of shaft [1] .

Use of finite element based formulation is the prevalent approach to analyzing the deformation of the rotating shaft. To analyze shafts with complicated geometries, or under large deformation, the use of solid finite element is typically required [2]. This, however, can lead to high computational costs, as a solid finite element model often consists of a very large number of degrees of freedom. Beam elements with a high number of degrees of freedom in the transversal directions, such as high-order beam element based on absolute nodal coordinate formulation (ANCF), are the alternative to solid element in the prediction of cross-section deformation of rotating shaft.

In the absolute nodal coordinate formulation, the nodal coordinates of beam and plate elements are defined using global position vector and components of the deformation gradient. Use of the deformation gradients in element transverse direction allows the description of shear and thickness deformation in the formulation. The first high-order elements to alleviate locking due to cross-section deformation were introduced by Matikainen et al. [3, 4, 5]. Shen et al. [6] introduced several high-order beam element models subjected to large deformation to characterize the cross-section deformation. Subsequently, Orzechowski and Shabana [7] studied the high-order beam element with 42 degrees of freedom originally proposed in [6]. They examined the high-order beam element with a variety of cross-section shapes, including a rectangular tube and an ellipse to investigate the warping effect. Recently, by comparing several low- and high-order beam elements, Ebel et al. [8] has demonstrated that in three- and four-node high-order beam elements with a rectangular cross-section, more-accurate results can be obtained compared to transversally linear beam elements.

This paper applies an ANCF based approach to the dynamic analysis of rotating shafts. The approach uses the high-order beam element denoted as 34X3 proposed by Ebel et al. [8]. This paper presents a number of static and dynamic benchmark tests, and their results are compared to the reference solutions from literature and the commercial finite elements code ANSYS. The introduced approach is found to be able to predict the cross-section deformation of a circular structure.

2 Kinematics of high-order ANCF beam element

This section reviews the kinematics of the employed element. This study employs a four-node high-order ANCF beam element with 120 degrees of freedom [8]. The nodal location is depicted in Fig. 1 in which $\boldsymbol{e}_i$ is the vector of nodal coordinates that includes positions and derivatives evaluated at the i^{th} node. The depicted nodal degrees of freedom can be also expressed in vector form as

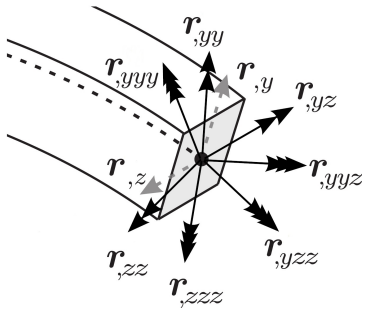

Fig. 1: Illustration of the employed ANCF beam element and its first- and high-order directional derivatives as degrees of freedom [8].

$$\boldsymbol{e}_i^{[34X3]} = \left[\boldsymbol{r}^{(i)\mathrm{T}} \quad \boldsymbol{r}_{,y}^{(i)\mathrm{T}} \quad \boldsymbol{r}_{,z}^{(i)\mathrm{T}} \quad \boldsymbol{r}_{,yz}^{(i)\mathrm{T}} \quad \boldsymbol{r}_{,yy}^{(i)\mathrm{T}} \quad \boldsymbol{r}_{,zz}^{(i)\mathrm{T}} \quad \boldsymbol{r}_{,yyz}^{(i)\mathrm{T}} \quad \boldsymbol{r}_{,yzz}^{(i)\mathrm{T}} \quad \boldsymbol{r}_{,yyy}^{(i)\mathrm{T}} \quad \boldsymbol{r}_{,zzz}^{(i)\mathrm{T}} \quad \right]^{\mathrm{T}}. \tag{1}$$

The element's polynomial basis is

$$\begin{aligned}\beta^{[34X3]} := [1, x, y, z, xy, xz, x^2, x^2y, x^2z, y^2, xy^2, x^2y^2, z^2, xz^2, z^2, yz, xyz, x^2y, x^3, x^3y \\ , x^3z, x^3yz, x^3y^2, x^3z^2, y^2z, xy^2z, x^2y^2z, x^3y^2z, yz^2, xyz^2, x^2yz^2, x^3yz^2, y^3, \\ xy^3, x^2y^3, x^3y^3, z^3, xz^3, x^2z^3, x^3z^3].\end{aligned}$$

In the ANCF, the position vector $\boldsymbol{r}$ of an arbitrary particle, can be expressed as follows:

$$\boldsymbol{r}(\boldsymbol{\xi}, t) = \boldsymbol{S}_{\mathrm{m}} \boldsymbol{e}(t)\,, \tag{2}$$

where $\boldsymbol{S}_{\mathrm{m}}$ is the shape function matrix containing 40 shape functions. Since the 34X3-element is isoparametric, the resulting shape functions can be given in both a physical coordinate system (x, y, z) and a bi-normalized local element coordinate system (ξ, η, ζ) with $\xi = \dfrac{x}{l_x}$, $\eta = \dfrac{y}{R}$ and $\zeta = \dfrac{z}{R}$, where l_x and R are the length and diameter of the beam element, respectively.

3 Equations of motion

The weak form of the equations of motion of an ANCF element can be expressed as

$$\int_V \rho \ddot{\boldsymbol{r}} \cdot \delta \boldsymbol{r}\, \mathrm{d}V + \int_V \boldsymbol{S} : \delta \boldsymbol{E}\, \mathrm{d}V - \int_V \boldsymbol{b} \cdot \delta \boldsymbol{r}\, \mathrm{d}V = 0\,, \tag{3}$$

where the first integral is associated with the inertia, the second integral is associated with the elastic forces, and the third integral concerns externally applied forces [9]. In Eq. (3), $\boldsymbol{S}$ is the second Piola-Kirchhoff stress tensor, $\boldsymbol{E}$ is the Green-Lagrange strain tensor, $\boldsymbol{b}$ stands for the vector of body forces and V is the integration domain over the element in the reference configuration. The present study employs three-dimensional elasticity in the form of the St. Venant-Kirchhoff material model that assumes a linear relationship as follows:

$$\boldsymbol{S} = \lambda\, \boldsymbol{I}\, \mathrm{tr}\,(\boldsymbol{E}) + 2G\,\boldsymbol{E}\,, \tag{4}$$

where λ and G are the 1^{st} Lamé elastic constant and shear modulus, respectively. The Green-Lagrange strain tensor is defined as

$$\boldsymbol{E} = \frac{1}{2}\left(\boldsymbol{C} - \boldsymbol{I}\right), \tag{5}$$

where $\boldsymbol{C}$ is the right Cauchy-Green strain tensor and can be expressed in terms of the deformation gradient $\boldsymbol{F}$ as

$$\boldsymbol{C} = \boldsymbol{F}^T \boldsymbol{F}\,. \tag{6}$$

As $\boldsymbol{r}$ defines the current position of an arbitrary particle and $\boldsymbol{\xi} = \begin{bmatrix}\xi & \eta & \zeta\end{bmatrix}^{\mathrm{T}}$, the deformation gradient $\boldsymbol{F}$ reads

$$\boldsymbol{F} := \frac{\partial \boldsymbol{r}}{\partial \boldsymbol{r}_0} = \frac{\partial \boldsymbol{r}}{\partial \boldsymbol{\xi}}\,\boldsymbol{J}^{-1}, \tag{7}$$

where $\boldsymbol{J} = \frac{\partial \boldsymbol{r}_0}{\partial \boldsymbol{\xi}}$ is the Jacobian matrix that provides a transformation between the physical and local coordinate systems. The vector of elastic forces of the i^{th} beam element is expressed as follows:

$$\boldsymbol{F}_e = l_x \int_A \boldsymbol{S} : \frac{\partial \boldsymbol{E}}{\partial \boldsymbol{e}}\, dA\,, \tag{8}$$

which holds for a circular cross-section with $A = (\eta, \zeta) : \eta^2 + \zeta^2 \leq R$. The integral of Eq. (8) is computed based on standard Gaussian quadrature formulas [10]. In case of circular cross-section

$$\int_A \boldsymbol{F}_e(\eta\,, \zeta)\, d\eta\, d\zeta = \pi \frac{R^2}{4} \sum_{i=1}^{n} w_i\, \boldsymbol{F}_e(\eta_i\,, \zeta_i)\,, \tag{9}$$

where n is the number of Gaussian points along cross-section axes (η, ζ) and w_i is weight of the i^{th} integration point.

4 Numerical examples

The numerical examples compare displacements based on the ANCF beam element and commercial finite element code ANSYS in static and dynamic cases. The tests are carried out using circular cross-section. A high-order ANCF beam element with 120 degrees of freedom is used, while ANSYS employs the quadratic 20-node solid element, SOLID186 in the solution of the numerical examples.

4.1 Simply supported beam

This section presents a bending test composed of a circular cross-section beam with simply supported boundary conditions. The beam is of the length $L = 2$ m and radius $r = 0.25$ m. Young's modulus and Poisson's ratio are set to be $E = 2.07 \times 10^{11}$ N/m^2 and $\nu = 0.3$, respectively. The surface force $F_y = -1.08 \times 10^9 / r\pi L$ N/m^2 is applied on the top surface of the beam. The elastic forces are computed using the Gaussian quadrature rule with an appropriate number of integration points. The simply supported boundary conditions in the ANCF beam are

described by constraining the first three nodal degrees of freedom at one end and the second and third degrees of freedom at the other end. The simply-supported boundary conditions in ANSYS are modeled using node-surface contact elements, CONTACT175 / TARGET170. To properly apply the vertical surface force, the surface effect element SURF154 is used in ANSYS. The force is applied to the underlying solid elements through the surface effect elements, SURF154. Tab. 1 shows the numerical results based on ANCF and ANSYS. The results obtained with the high-order ANCF element give converged solutions with 32 beam elements. The displacement of the selected point located in the middle of the top surface of the beam is in good agreement with ANSYS.

Tab. 1: Comparison of displacements of the top surface point of the beam undergoing bending using element 34X3 against the displacements given by SOLID186 in ANSYS.

Number of elements	x_{top} $[m]$	y_{top} $[m]$
2	−0.02088	−0.18468
4	−0.01990	−0.18158
8	−0.01962	−0.18075
16	−0.01954	−0.18052
32	−0.01951	−0.18043
96×24×24 (SOLID186)	−0.01944	−0.19095

4.2 Rotating shaft

This section analyzes the dynamic response of a flexible shaft supported at its ends by bearings. The shaft is connected to the ground by a revolute joint at one end and a cylindrical joint at the other end. The shaft undergoes rotation with angular velocity Ω, defined using a smoothed ramp function from zero at time $t = 0$ s to $\Omega(t) = 5000\,\text{RPM}$ at $t = 2$ s, as illustrated in Fig. 2. At the initial time, the shaft is at rest. The length of the shaft is $L = 2\,\text{m}$ and the shaft is made of steel with density of $\rho = 7850\,\text{kg/m}^3$, Young's modulus of $E = 2.10 \times 10^{11}\,\text{N/m}^2$, and Poisson's ratio of $\nu = 0.3$. The cross-section is circular with a radius of $r = 0.1\,\text{m}$. An analytical formula for the

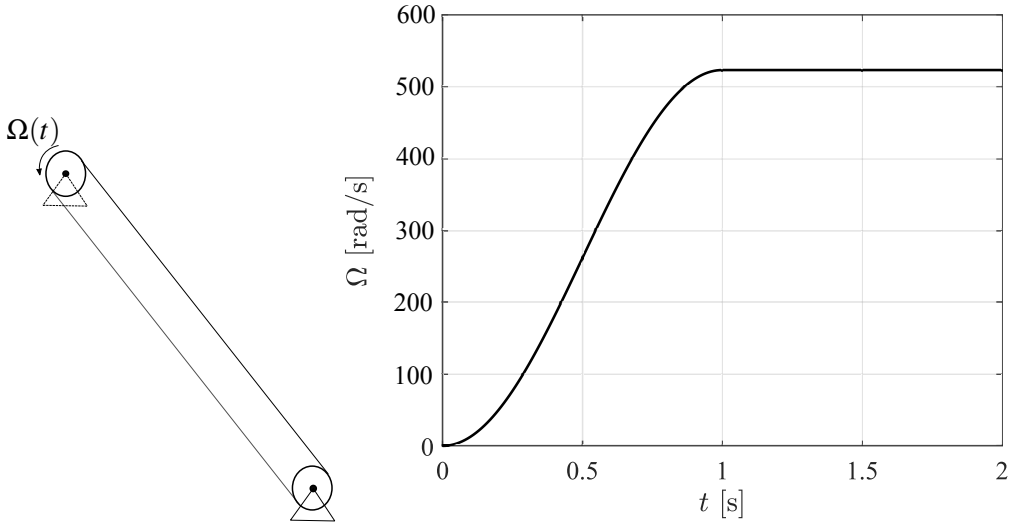

Fig. 2: Rotating shaft with applied angular velocity as ramp function of time

radial expansion of a solid cylinder [11] can be expressed as:

$$\Delta r = \frac{\rho \Omega^2 (1-\nu) r^3}{4E}, \tag{10}$$

where ρ is density, ν is Poisson's ratio, E is Young's modulus, Ω is the rotational frequency, and r is the radius of the shaft. According to Eq. (10), radial expansion Δr is proportional to the square of the rotational frequency Ω.

The flexible shaft is also modeled by commercial finite element software ANSYS using 3D solid element type SOLID186. Fig. 2 depicts the values of the angular velocity during simulation. A non-linear dynamic transient analysis was performed within the time span of 2 s, using a time step of 0.02 s. The boundary conditions are applied at the pilot nodes of both ends of the shaft to define the revolute and cylindrical joints. The two pilot nodes belong to node-surface contact elements CONTACT175 / TARGET170. Tab. 2 compares the numerical values obtained for radial displacement by ANSYS and the ANCF beam element. The ANCF result shows relatively good agreement with the value given by Eq. (10), even with only one high-order element. Note that applying boundary conditions on the center nodes instead of the whole areas prevents the cross-section from being constrained, which would lead to non-uniform radial expansion. Because of the constant mass matrix of the element in ANCF beam formulation, the centrifugal and Coriolis inertia forces are identically equal to zero [12, 13].

Tab. 2: Comparison between the resulting radial cross-section expansion obtained by ANSYS, ANCF and analytical approach in Eq. (10)

Analysis approach	Δr [μm]
Analytical	1.7934
Finite Elements (ANSYS)	1.8177
ANCF Beam 34X3	2.0178

5 Conclusions

This paper examined the high-order ANCF beam element originally introduced by Ebel et al. [8] in rotating shaft applications. The four-node beam element was applied to a number of benchmark tests to investigate its performance. This study examined the element in static and dynamic tests. The capability of the element to predict cross-sectional deformation and large displacements and accurately capture the cross-section expansion in a rotating shaft was validated. As demonstrated by numerical examples, the high-order beam element can capture the complicated cross section deformation more-accurately than the low-order ANCF beam element introduced by Nachbagauer et al. [14, 15]. Therefore, the ANCF beam element can be applied to the dynamic analysis of high-speed rotors.

References

[1] J. Wang, V.-V. Hurskainen, M. K. Matikainen, J. Sopanen, and A. Mikkola, "On the dynamic analysis of rotating shafts using nonlinear superelement and absolute nodal coordinate formulations," *Advances in Mechanical Engineering*, vol. 9, no. 11, pp. 1–14, 2017.

[2] K. Yoon, Y. Lee, and P.-S. Lee, "A continuum mechanics based 3-D beam finite element with warping displacements and its modeling capabilities," *Structural Engineering and Mechanics*, vol. 43, no. 4, pp. 411–437, 2012.

[3] M. K. Matikainen, O. Dmitrochenko, and A. Mikkola, "Beam elements with trapezoidal cross section deformation modes based on the absolute nodal coordinate formulation," in *International Conference of Numerical Analysis and Applied Mathematics*, (Rhodes, Greece), pp. 1266–1270, 19–25 September 2010.

[4] M. K. Matikainen, O. Dmitrochenko, and A. Mikkola, "Higher-order beam elements based on the absolute nodal coordinate formulation," in *Multibody System Dynamics, ECCOMAS Thematic Conference*, (Brussels,Belgium), 4-7 July 2011.

[5] M. K. Matikainen, A. I. Valkeapää, A. M. Mikkola, and A. Schwab, "A study of moderately thick quadrilateral plate elements based on the absolute nodal coordinate formulation," *Multibody System Dynamics*, vol. 31, no. 3, pp. 309–338, 2014.

[6] Z. Shen, P. Li, C. Liu, and G. Hu, "A finite element beam model including cross-section distortion in the absolute nodal coordinate formulation," *Nonlinear Dynamics*, vol. 77, no. 3, pp. 1019–1033, 2014.

[7] G. Orzechowski and A. A. Shabana, "Analysis of warping deformation modes using higher order ANCF beam element," *Journal of Sound and Vibration*, vol. 77, no. 3, pp. 1019–1033, 2015.

[8] H. Ebel, M. K. Matikainen, V.-V. Hurskainen, and A. Mikkola, "Higher-order beam elements based on the absolute nodal coordinate formulation for three-dimensional elasticity," *Nonlinear Dynamics*, vol. 88, no. 2, pp. 1075–1091, 2017.

[9] J. Gerstmayr and M. K. Matikainen, "Analysis of stress and strain in the absolute nodal coordinate formulation," *Mechanics Based Design of Structures and Machines*, vol. 34, no. 4, pp. 409–430, 2006.

[10] M. Abramowitz and I. A. Stegun, *Handbook of mathematical function*. Washington, D.C.: United States Department of Commerce, National Institute of Standards and Technology, 1964.

[11] P. Günther, F. Dreier, T. Pfister, J. Czarske, T. Haupt, and W. Hufenbach, "Measurement of radial expansion and tumbling motion of a high-speed rotor using an optical sensor system," *Mechanical Systems and Signal Processing*, vol. 25, no. 1, pp. 319–330, 2011.

[12] R. Y. Yakoub and A. A. Shabana, "Three dimensional absolute nodal coordinate formulation for beam elements: implementation and applications," *Journal of Mechanical Design*, vol. 123, no. 4, pp. 614–621, 2001.

[13] A. A. Shabana and R. Y. Yakoub, "Three dimensional absolute nodal coordinate formulation for beam elements: theory," *Journal of Mechanical Design*, vol. 123, no. 4, pp. 606–613, 2001.

[14] K. Nachbagauer, A. S. Pechstein, H. Irschik, and J. Gerstmayr, "A new locking-free formulation for planar, shear deformable, linear and quadratic beam finite elements based on the absolute nodal coordinate formulation," *Multibody System Dynamics*, vol. 26, no. 3, pp. 245–263, 2011.

[15] K. Nachbagauer, P. Gruber, and J. Gerstmayr, "A 3D shear deformable finite element based on the absolute nodal coordinate formulation," in *Multibody System Dynamics* (J.-C. Samin and P. Fisette, eds.), vol. 28 of *Computational Methods in Applied Sciences*, pp. 77–96, Springer Netherlands, 2013.